Supplement of Atmos. Chem. Phys., 25, 17651–17665, 2025
https://doi.org/10.5194/acp-25-17651-2025-supplement

Atmospheric Chemistry and Physics
Open Access
EGU

Supplement of

Temperature and stagnation effects on ozone sensitivity to NO_x and VOC: an adjoint modeling study in central California

Yuhan Wang et al.

Correspondence to: Ling Jin (ljin@lbl.gov) and Robert A. Harley (harley@ce.berkeley.edu)

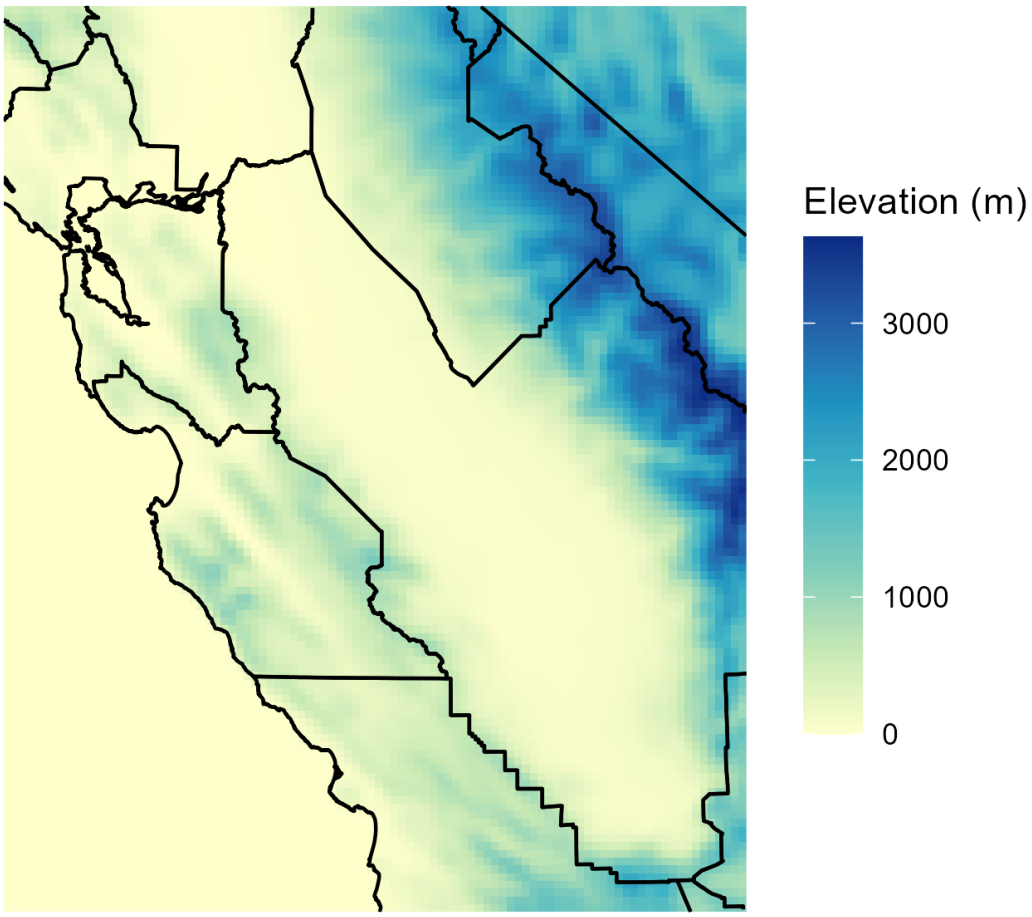

Figure S1. Surface altitude in the modeling domain.

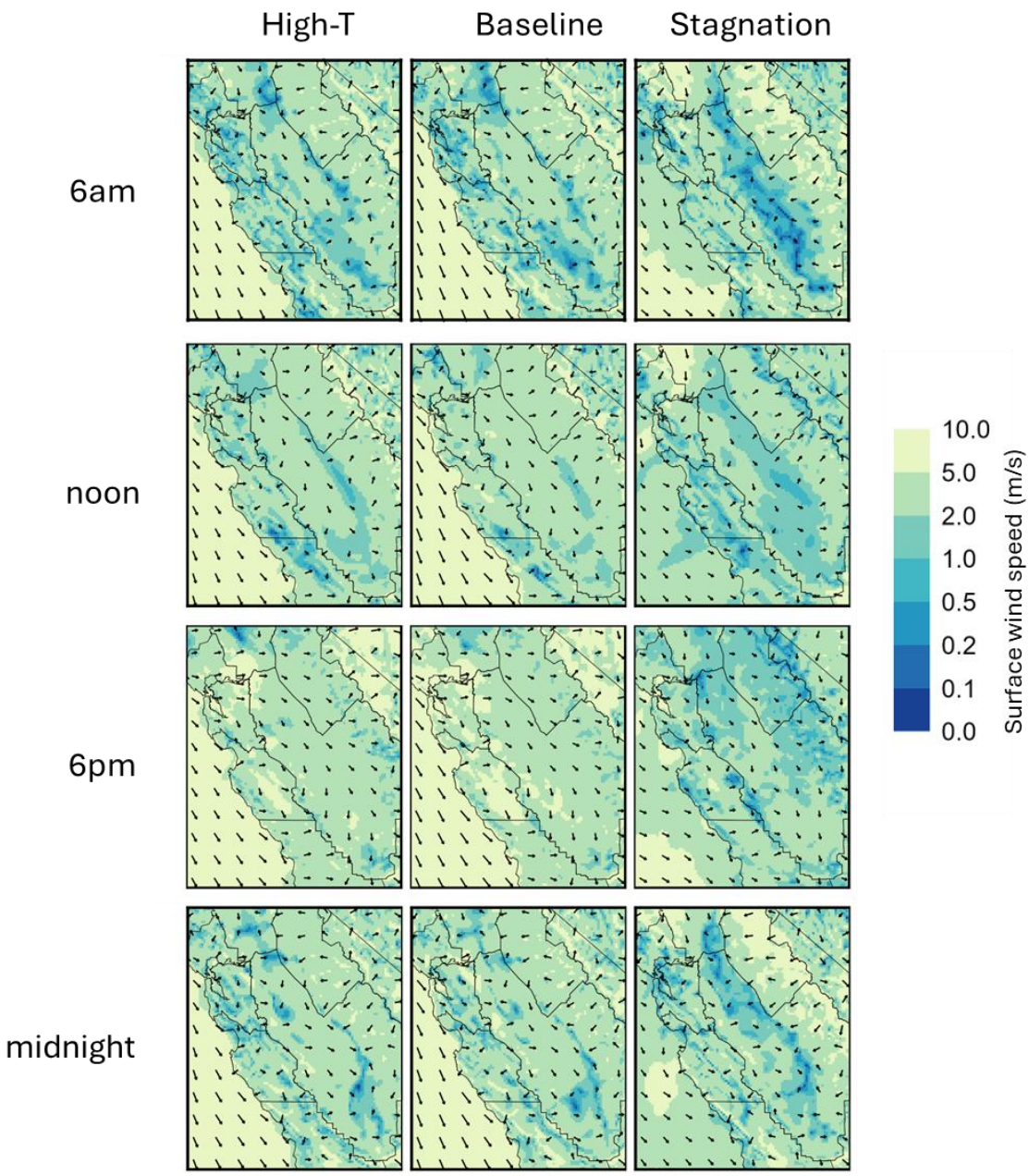

Figure S2. Surface wind fields at different hour of day (6am, noon, 6pm, midnight) under high-T (left column), baseline (middle), and stagnation (right column) meteorological scenarios. Arrow represents wind direction, and color indicates wind speed.

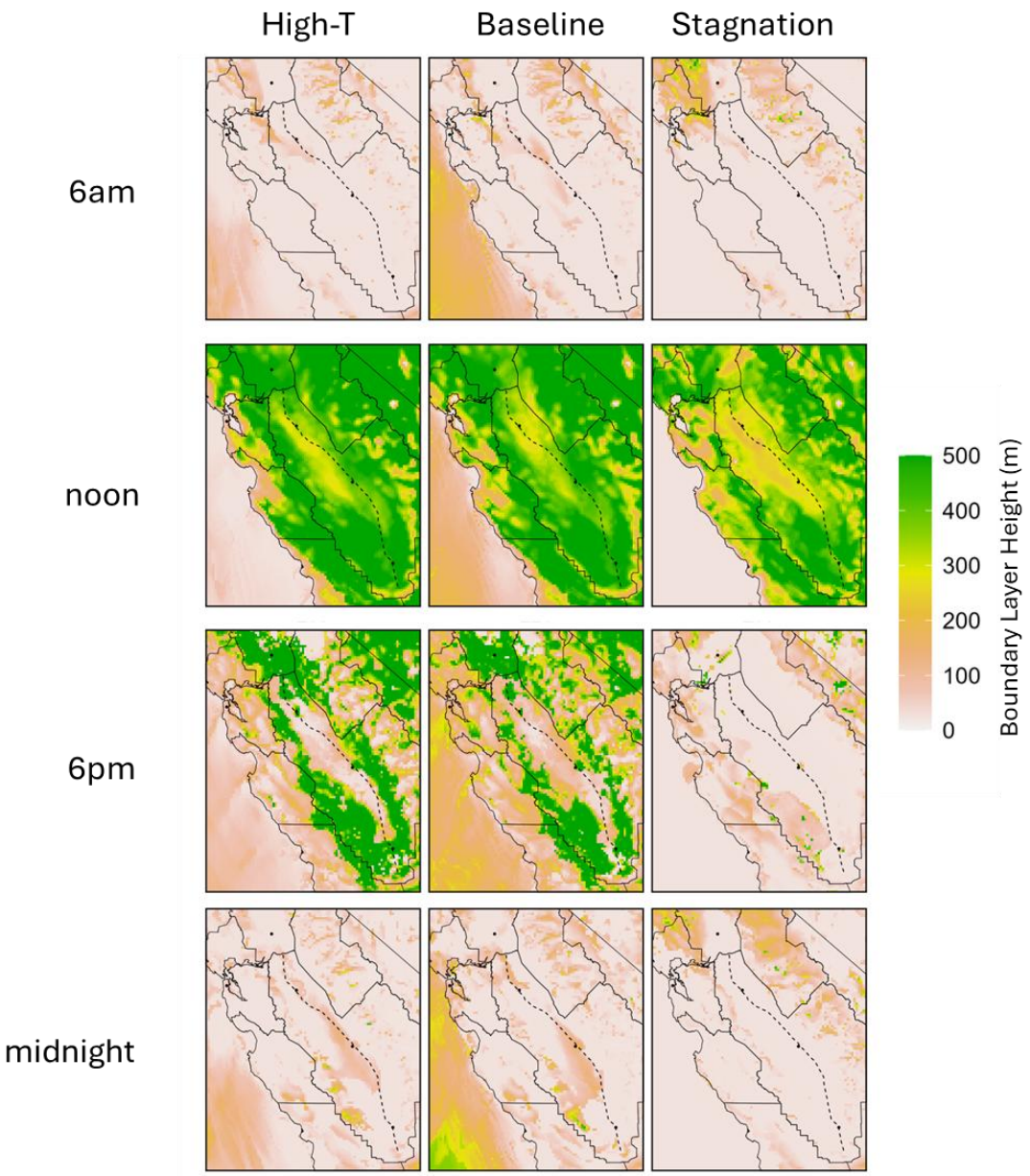

Figure S3. Planetary Boundary Layer (PBL) heights at different hour of day (6am, noon, 6pm, midnight) under high-T (left column), baseline (middle), and stagnation (right column) meteorological scenarios.

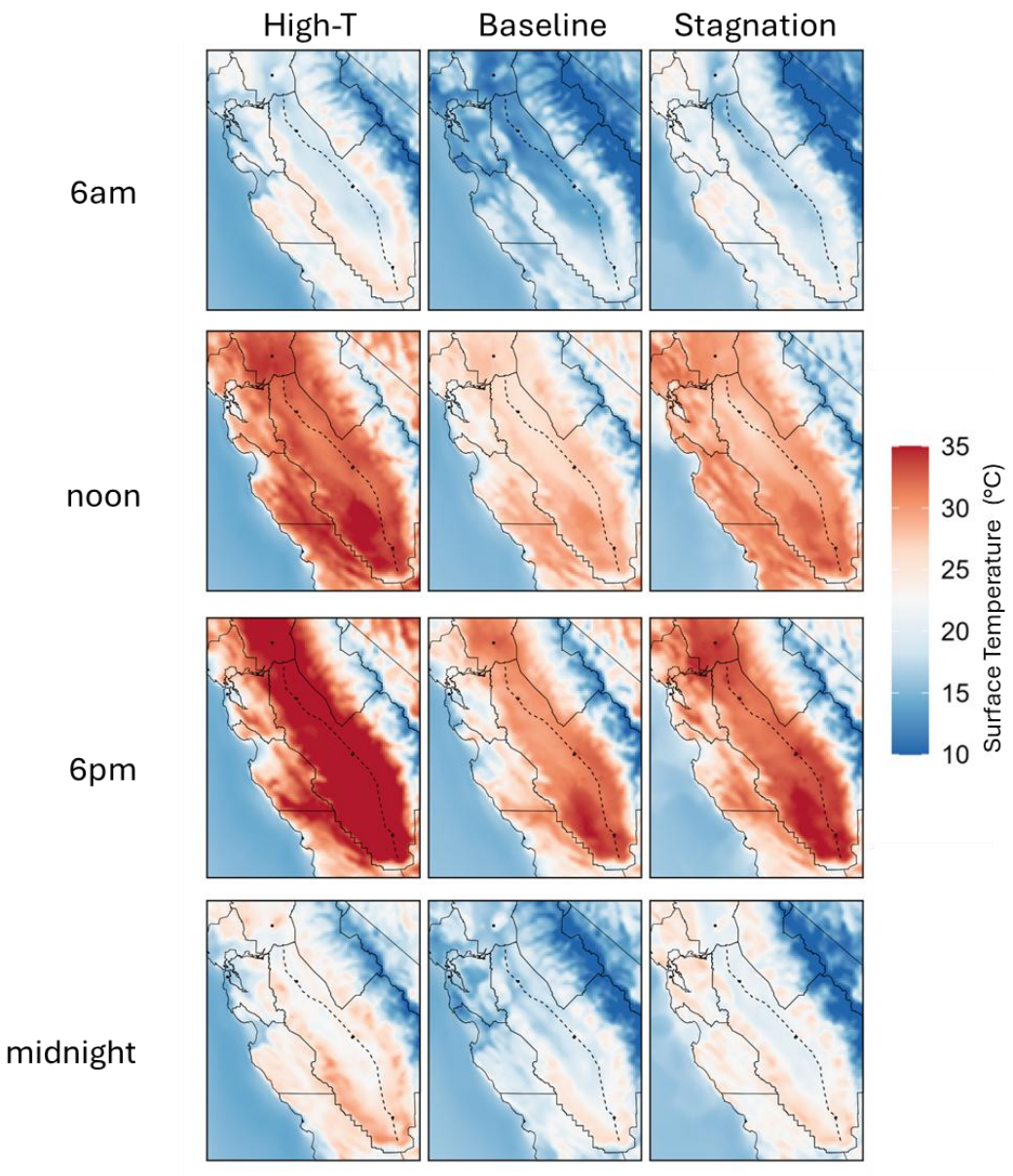

Figure S4. Surface temperature fields at different hour of day (6am, noon, 6pm, midnight) under high-T (left column), baseline (middle), and stagnation (right column) meteorological scenarios.

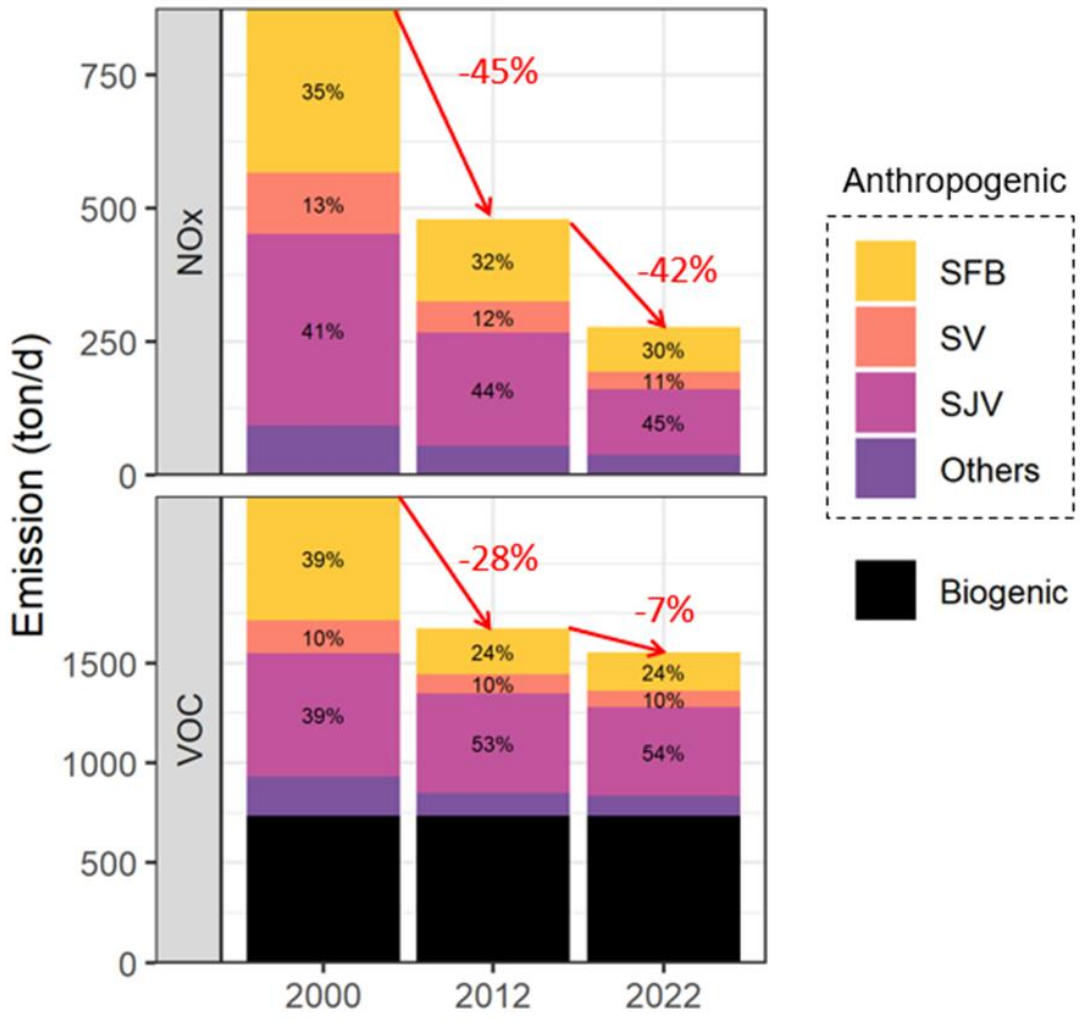

Figure S5. Domainwide emission sums of NO_x (top panel) and VOC (bottom panel). Anthropoegnic NO_x and VOC emissions are colored by source region, and biogenic emissions are colored in black.

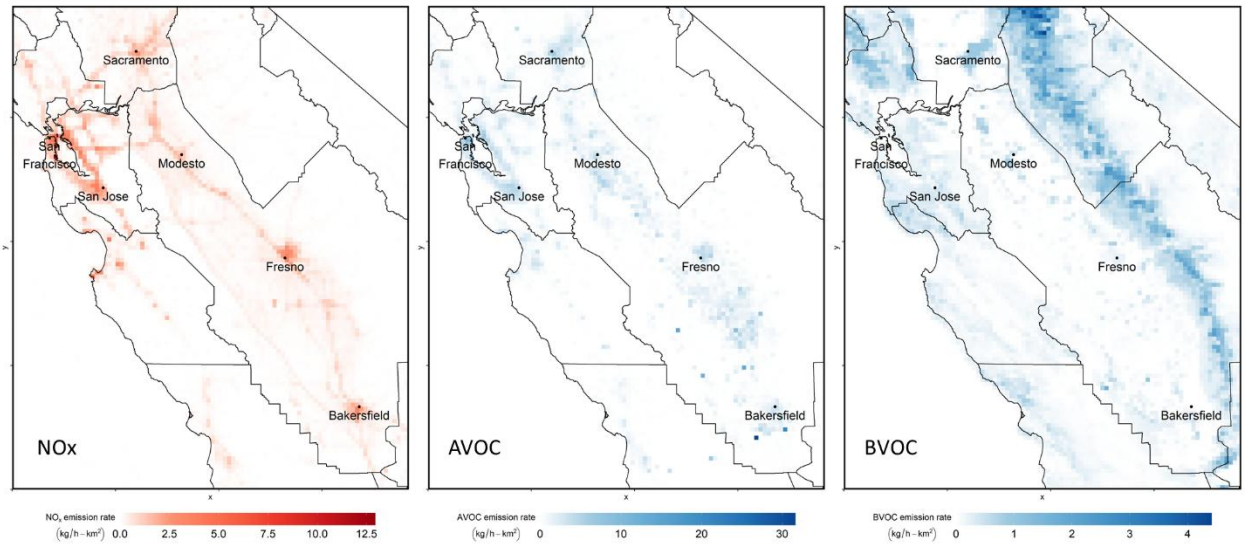

Figure S6. Spatial distributions of NO_x (left), anthropogenic VOC (middle) and biogenic VOC (right) emissions in year 2012. Major cities in the domain are labeled.

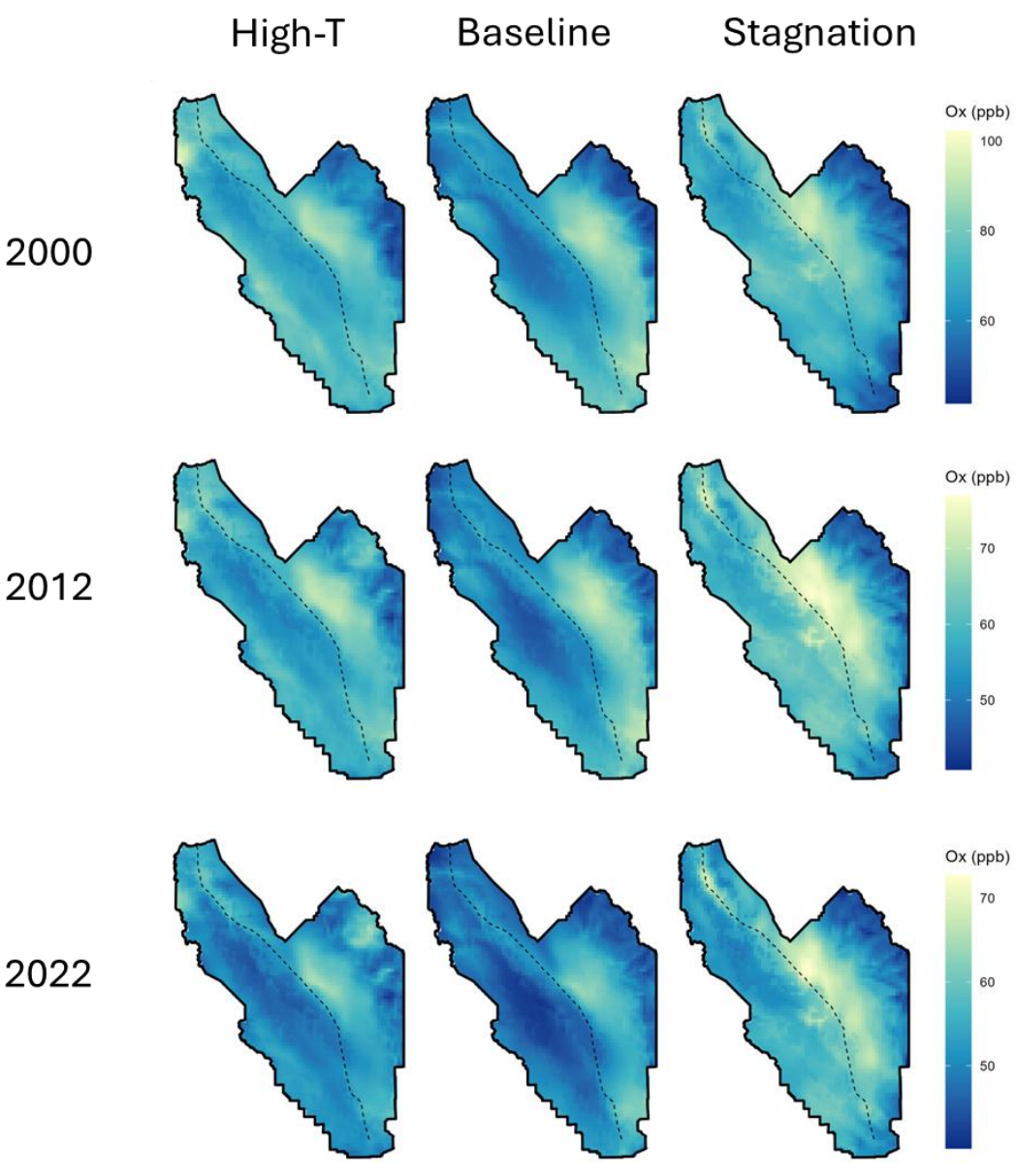

Figure S7. Spatial distributions of simulated 8-hour (10am-6pm) Odd Oxygen ($O_x = O_3+NO_2$) concentration inside the San Joaquin Valley. Note that color legends vary for different years.

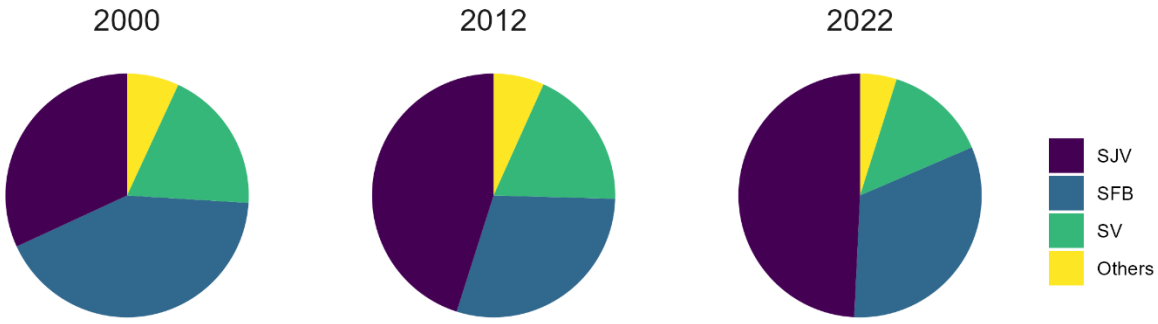

Figure S8. Breakdown of anthropogenic contributions by source region: San Joaquin Valley (SJV), San Francisco Bay (SFB), Sacramento Valley (SV), and other air basins (e.g., North Central Coast, South Central Coast, Mountain Counties). Results shown are for baseline meteorology.

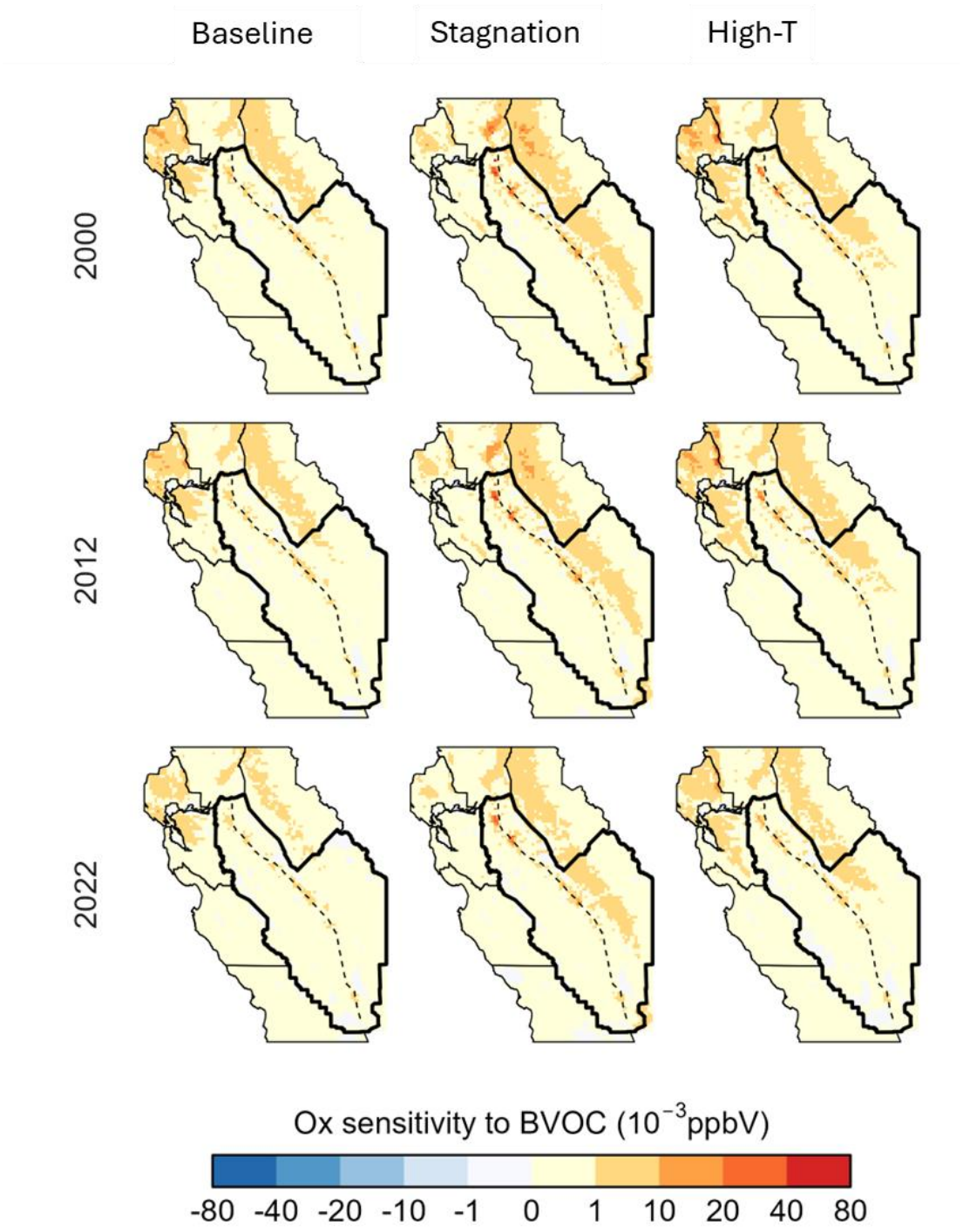

Figure S9. Spatial distribution of sensitivity to biogenic VOC (BVOC) under varying emission and meteorology scenarios.

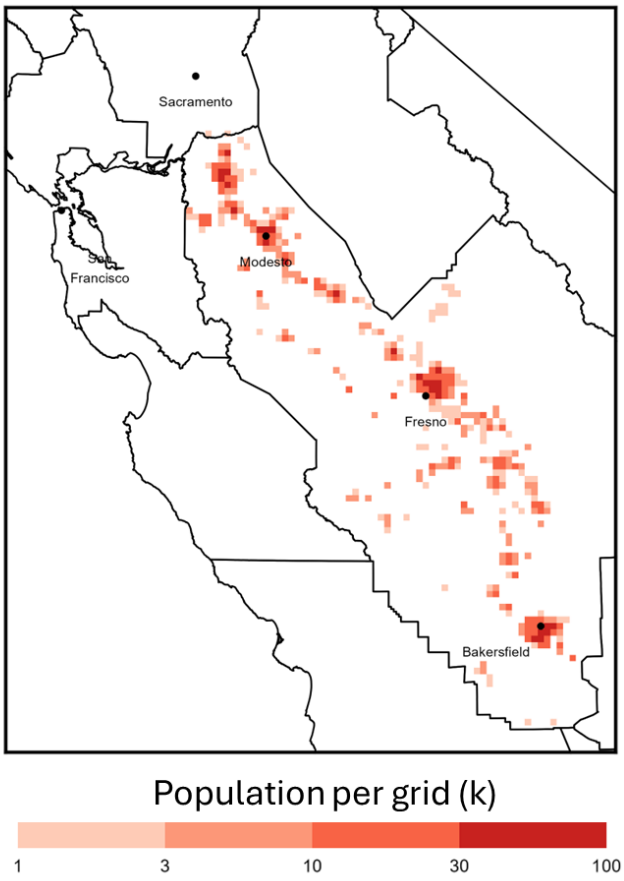

Figure S10. Population distribution inside the San Joaquin Valley.

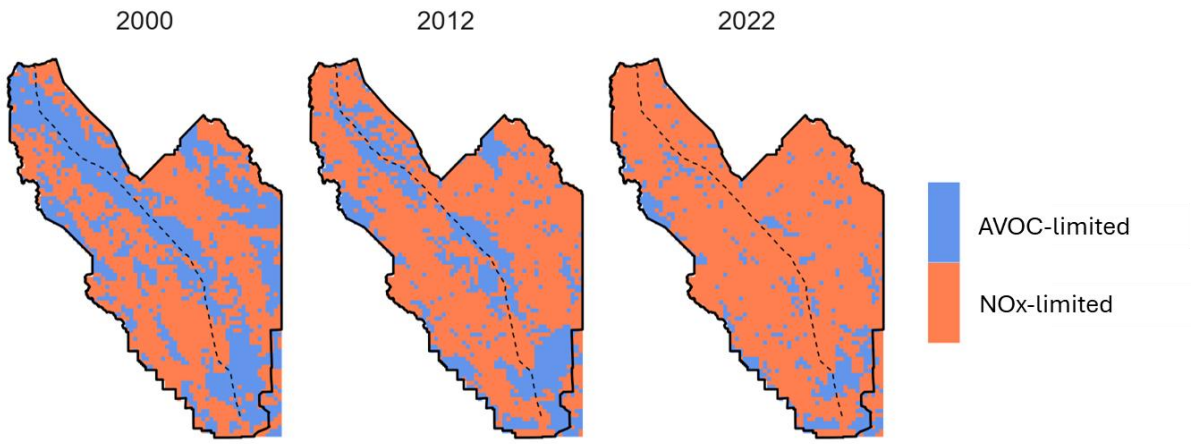

Figure S11. Preferred precursor type to target inside the San Joaquin Valley (SJV). A grid cell is colored in blue if its anthropogenic VOC (AVOC) contribution to SJV O_x outweighs NO_x contribution, and colored in orange otherwise. Results shown are for baseline meteorology.

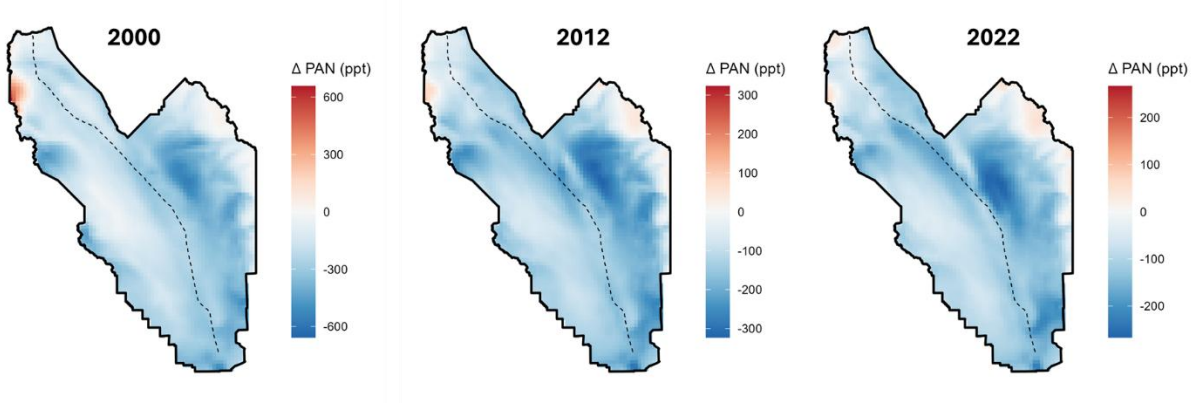

Figure S12. Changes in PAN concentration under high-T conditions, relative to baseline, for the 2000, 2012, and 2022 emission scenarios.

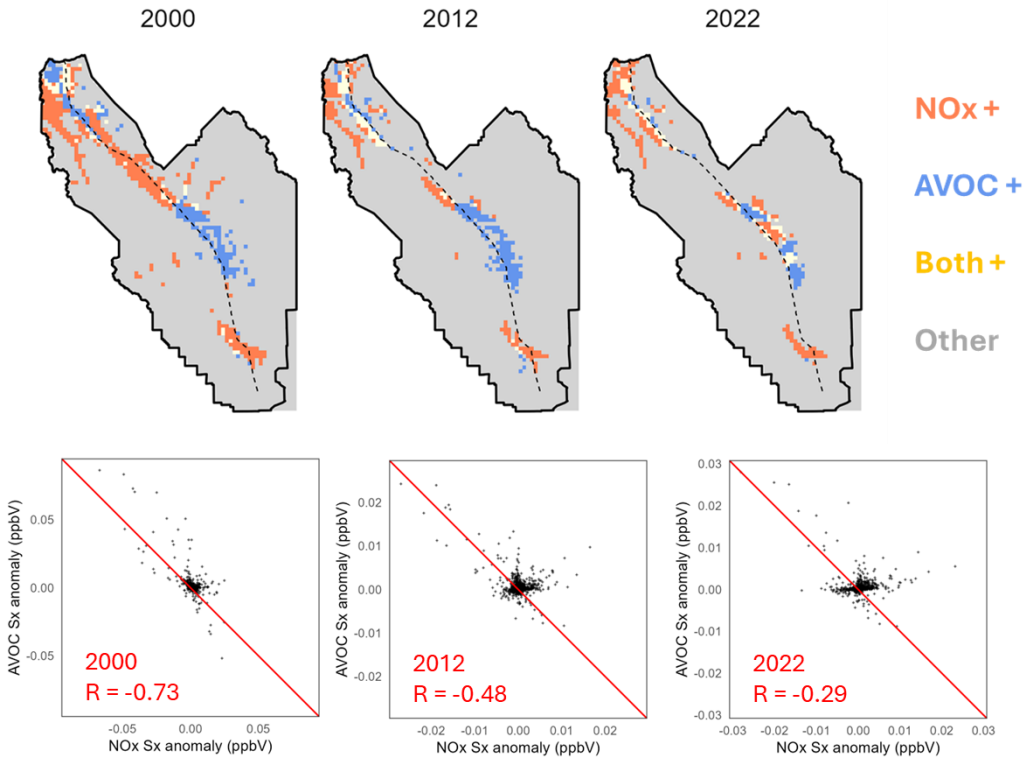

Figure S13. Maps (top row) show where high-T conditions increase sensitivity to NOx (orange), anthropogenic VOC (blue), or both (yellow). Gray-colored portions indicate source areas where sensitivity changes are negligible. Scatter plots (bottom row) compare changes in sensitivity to NOx versus AVOC at grid cell level, when meteorology switches from baseline to high-T.

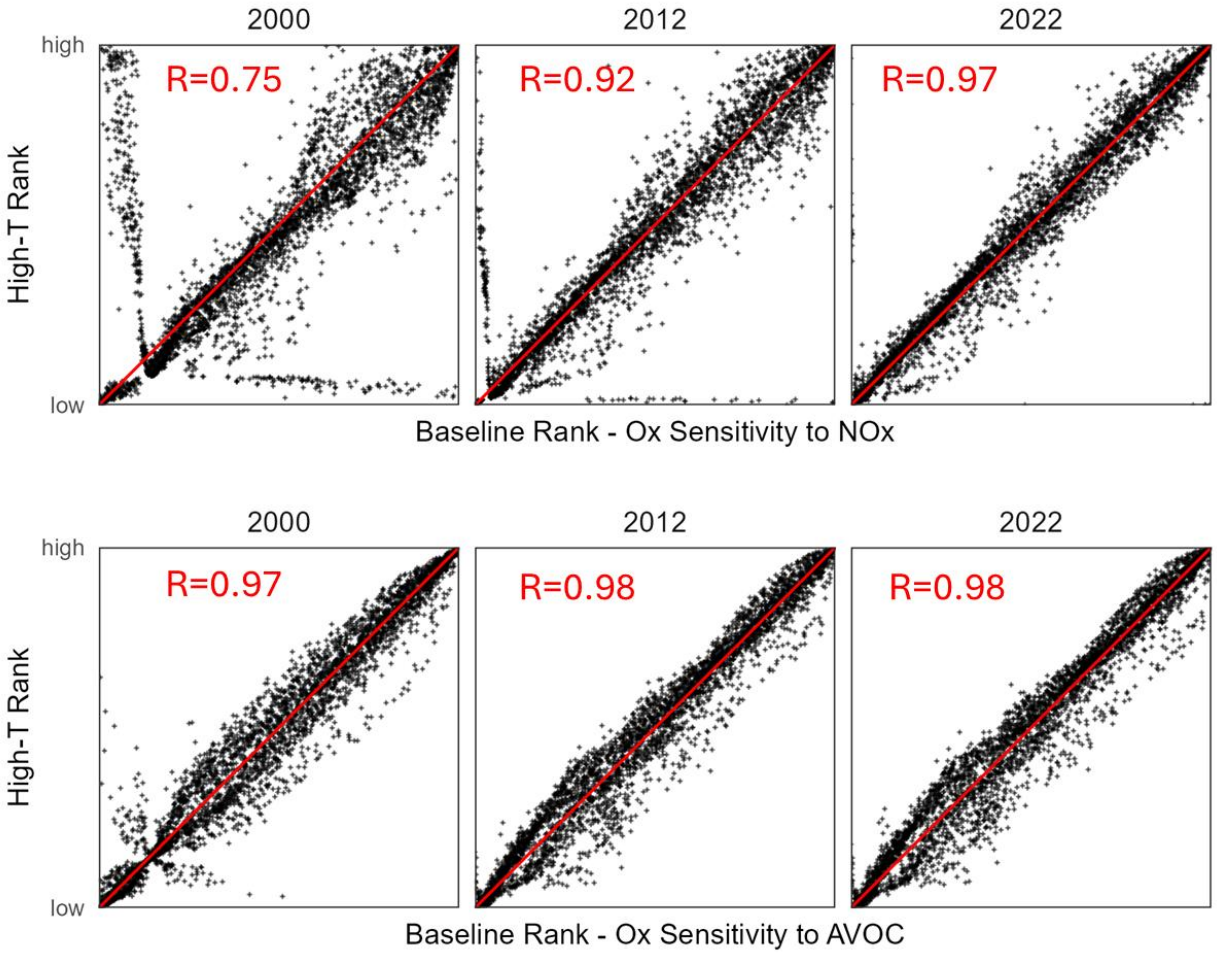

Figure S14. Baseline versus high-T rankings of all San Joaquin Valley (SJV) grid cells based on their individual NOx (top) and AVOC (bottom) contributions to the SJV Ox receptor. Higher rankings indicate greater effectiveness when targeting these source areas for emission control. Large correlation coefficients reflect strong consistency in optimal source control strategies between baseline and high-T conditions.

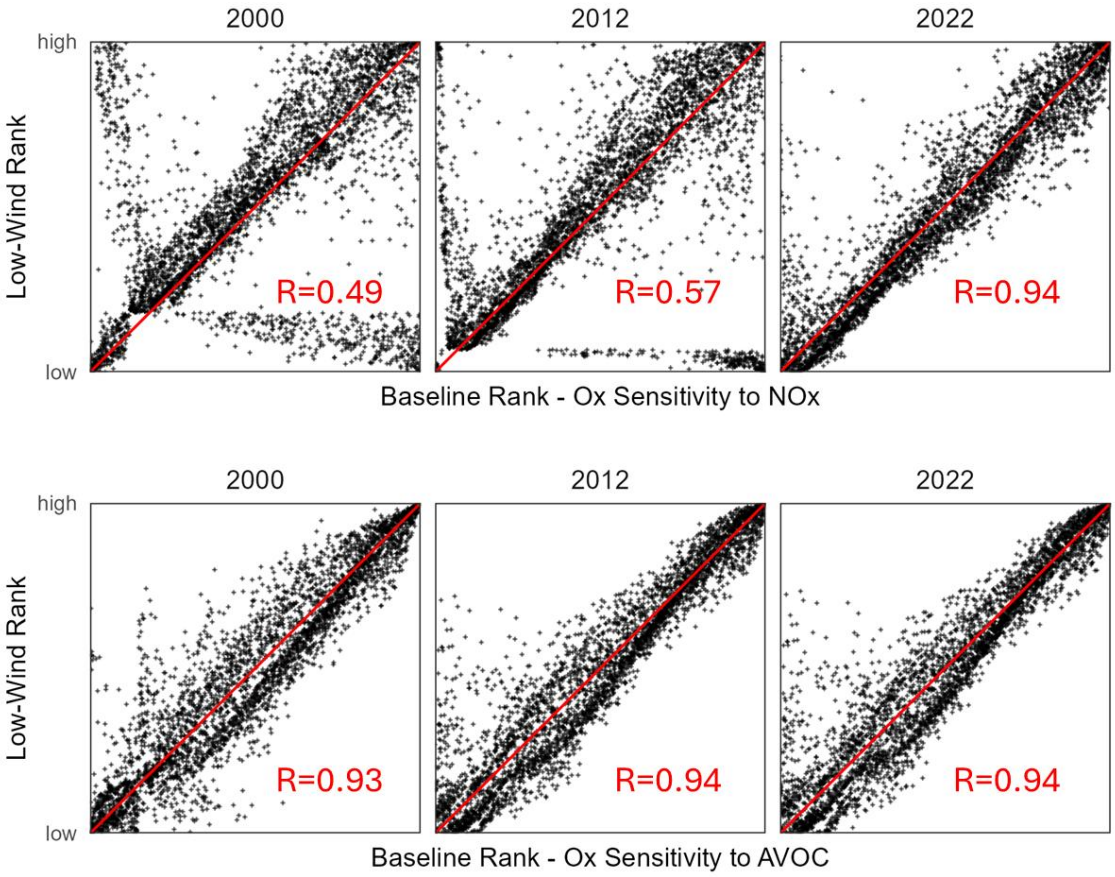

Figure S15. Baseline versus stagnation rankings of all San Joaquin Valley (SJV) grid cells based on their individual NOx (top) and AVOC (bottom) contributions to the SJV Ox receptor. Higher rankings indicate greater effectiveness when targeting these source areas for emission control. Small correlation coefficients for NO_x reflect limited consistency in optimal source control strategies between baseline and stagnant conditions.